Viscous Lower Crust and Lower Crustal Shear Strain Localization in the Tibetan Plateau: From the Constraint of the GPS Velocity Field

LU Shikuo

Abstract—On the assumption that the GPS（Global Positioning System）velocity field is affected by the interseismic elastic deformation of the upper crust to a great degree, under the constraint of the existing GPS data, by the numerical simulation method we construct the viscoelastic mechanical models to analyse the rationality of the explanation to the Tibetan present-day crustal movement by the two different deformation mechanisms in the deep continental lithosphere, such as the viscous flow in the lower crust and the shear strain localization in the deep fault zones, in this paper. Numerical experiments show that the present-day crustal movement in the different regions of the Tibetan plateau may be attributed to the different geodynamic mechanisms. In the Tibetan southeastern area, although the shear strain localization in the deep fault zones could not be rejected, the viscosity of the lower crust should be much lower in order to diminish the model's prediction error. In the central-northern and northeastern areas of the Tibetan plateau, the GPS velocity field is interpreted much better by the shear strain localization in the deep fault zones, implying that the actual active faults may incise down deeply in these areas. Ignoring the lateral change of the viscosity in the lower crust, the preferred model by which the GPS velocity field could be accounted for with a first-order similarity yields an estimate of 10^{22}—5×10^{22}Pa·s for the mean viscosity of the Tibetan lower crust, and an estimate of about 10^{21}Pa·s for that of the deep fault zones. Due to the high elevation and the lower viscosity of the lower crust, the gravity plays an important role on the present-day movement of the Tibetan plateau.

Keywords—ductile flow in the lower crust, GPS data, numerical experiment, shear strain localization in deep fault zones, Tibetan plateau

I. INTRODUCTION

Currently, the pattern of the continental deformation is a subject of considerable controversy. Studies of the depth extent of rupture in large continental earthquakes show that seismic slip on these faults occurs mainly in the upper 10-20 km of the crust[1,2]. The interseismic elastic strain accumulation in the seismogenic upper crust is balanced by the coseismic strain release, so the upper crust deforms discontinuously over the long term, with slip on faults accommodating the relative motions of crustal blocks[3,4]. There are two distinct models as to how deformation is accommodated in the lower part of the continental lithosphere.

In one view, the faults cut through the entire continental lithosphere, as they do through oceanic lithosphere. Deformation occurs in the lower layer by stable frictional sliding on faults[5-7]. In this case, the relative motion among different blocks is controlled by stresses on their edges and the mechanical character of the fault zones. In an alternative view, the lower part of the lithosphere deforms in a distributed fashion, applying shear tractions to the base of the brittle upper crust[8-10]. In recent years, some geophysical explorations reveal that the lower crust might be weak mechanically and flows viscously[11,12], and at the same time, there is ductile strain localization in the narrow zones beneath the frictional sliding faults[13,14]. This implies that the actual deformation pattern in the lower part of the lithosphere might be the synthesis of the former two simplified models.

As an ideal natural geodynamic laboratory, several competing models for the uplift and deformation of Tibet have been in dispute, each with different implications for the lower part of the Tibetan lithosphere[15-19]. With the rapid development of the global positioning technology, a lot of GPS data have been accumulated so far in the Qinghai-Xizang area[20-27], which image the interseismic deformation to a great degree due to the short time of observation and the extensive spreading of earthquakes in this area [28,29]. Similar to the former two simplified models, some scientists interpret the geodetic data near an active fault by the fault model where the fault is locked in the upper crust and slides stably in the lower layer of the lithosphere[7,24,28,30]. Another scientists emphasize that the interseismic deformation of the seismogenic upper crust is controlled by the distributed flow of the lower crust [28,29]. Here, in terms of the existing GPS data(Fig.1) and by means of the numerical simulation method, the goal of this paper is to investigate the relative rationality of the explanation to the Tibetan present-day crustal movement by the two different deformation mechanisms in the deep continental crust, either the viscous flow in the lower crust or the lower crustal shear strain localization in the deep fault zones. Based on this, finally we propose a dynamical model of the Tibetan present-day crustal movement and point out the feature of the Tibetan crustal viscosity.

DOI: 10.5176/2335-6774_1.1.10

II. FEATURE OF THE GPS DATA IN THE TIBETAN AREA

Since 1990s, a few of regional GPS observation networks[20-27] have been set up in the Tibet and its surrounding area in order to investigate the active tectonic characteristics of this region. Wang et al.(2001) and Zhang et al.(2004) collect and unify the existing GPS original observation data of the different regions, obtaining 354 and 553 observation stations' data respectively. Here the data depending on Zhang et al.(2004) (Figure 1) is adopted, which being from the net station http://www.geosociety.org/pubs/ft2004.htm. According to the research of reference [31],the distribution feature of the active faults in the Tibetan area is also shown in Figure 1.

Fig.1 Simplified active tectonic map of the Tibetan plateau. The dashed curve lines show the locations of the active faults based on Deng et al.(2002). The straight lines shows the velocity vectors of the GPS stations referring to Zhang et al.(2004), and the raw data are obtained from http://www.geosociety.org/pubs/ft2004.htm. The shade of gray denotes the elevation according to the global ETOPO5 data.

III. MODEL CONSTRUCTION

A. Geometry and boundary conditions

For convenience, we set up our geometrical model as a rectangle in the x-y plane, being 3200 km long and 2000 km wide(Fig. 2). It extends from the 74°E to the 108°E along the X axis and from 22.5°N to 40.5°N along the Y axis. Referring to the features of the active faults in the Tibetan Plateau[31,32], the model takes some major active faults into account. With the temperature and the surrounding pressure increasing, there is a transition between discrete frictional slip on a fault and bulk, continuum flow in a ductile shear zone[14]. Here, we assume that the fault cut through the whole model and behavior as a ductile shear zone in the lower crust. All the faults are simplified as upright deformation zones and are 50 km wide horiazontally.

Fig.2 Geometry and boundary conditions of the mechanical model. The model covers the same area as that shown in Fig.1. The curve lines represent the major active faults. The thin and thick straight lines with an arrow represent the velocity vectors of the GPS stations and the velocity boundary conditions, respectively. The northwestern boundary is set to slide freely along the S-N direction,and is constrained along E-W direction. The southeastern boundary is subjected to the lithostatic pressure laterally. A, B and C represent three subareas, which are used to evaluate the model.

The whole model is submitted to earth gravity and in a first step an initial long-wavelength（50km×50km）topography is assumed according to the global ETOPO5 data. Due to the gravity compensation isostatically, the thickness of the model's crust varies between 35 km and 70 km, depending on crustal （ ρc=2800kg/m3 ） and mental density(ρm=3300kg/m3). The base of the model is subjected to hydrostatic forces arising from a fluid mantle. We do not consider the Earth Sphericity.

As a primary factor to result in the Tibetan deformation[33], it is shown by GPS data that the Indian plate moves to the northeast(N19°-22°E) almost as a whole at a rate of about 36-38mm/yr[26], which is consistent with the reestimated plate motion model averaged over the past 3 Myr[34], suggesting that the relative motion pattern between the Tibet and its surrounding regions change little in the past 3 Myr. Thus, referring to the GPS data, we set the boundary conditions of the model as those shown in fig.2. Considering that the value and direction of the velocity assumed in the northern and eastern boundaries might have some deviation from the actual crustal movement, we test the effect of their little changes on the numerical experimental results and find that the experimental results are not sensitive to a little change of the northern and eastern boundary velocities of the model.

B. Rheology of the continental lithosphere

A linear Maxwell viscoelastic law[35] is adopted to fit the strain rate dependent power law rheology given by laboratory experiments for continental lithosphere. Since the focal depths of the shallow-focus earthquakes is commonly shallower than 15km[1,2], the rheology of the model is set to be elastic in the upper crust(lower than 15 km) and vicoelastic in the lower crust. Here, we pay more attention to the interseismic deformation and so ignore the brittle failure or plastic deformation beyond the elastic limit in the upper crust. In the course of the experiments, the deformation of the whole model is assumed to obey the linear Maxwell viscoelastic law and the pure elastic deformation of the upper crust is guaranteed by adopting a large viscosity 10^{28}Pa·s. We suppose different viscosities for the lower crust of the Tibet, the lower crust of the surrounding blocks and the deep fault zones, and test their effects on the velocity field of the Tibetan present-day crustal movement. Although the rock viscosity depends on temperature and pressure strongly, we choose to use a constant viscosity for the lower crust so as to simplify the forthcoming discussion.

IV. EXPERIMENTS AND RESULTS

The numerical experiments are done with the ADELI Geomechanical software provided by Chery and Hassani[36]. In the numerical experiments, the relaxation time associated with the lowest viscosity value ($\eta = 10^{20}$Pa·s) is about 30-40 years, we choose a time step of 0.1 year for all calculations during a 300 years long interseismic period.

In order to evaluate the model's result, we select three subregions(A、B、C) from the whole research area (Fig.2） and compute the root mean squares (RMS) of the model prediction errors of the directions as well as values of the GPS station velocities in each subregion, respectively. The model is evaluated mainly based on the root mean square of its prediction errors of the directions of the GPS station velocities. The velocities of the GPS stations outside the three

subregions are not used because those stations are close to the boundary of the Indian and Eurasian continents, where the main boundary thrust is simplified as a upright fault.

A. Effect of the lower crustal viscosity on the Tibetan present-day crustal movement

Firstly, we test the influence of the lower crustal ductile flow on the GPS velocity field. In this kind of experiments, only the discrepancy between the lower crustal viscosity of the Tibetan plateau and that of the surrounding blocks is dealed with, ignoring the lower crustal shear strain localization in the deep fault zones. Viscosity values between 10^{21} and 10^{26}Pa·s are tested for the Tibetan lower crust that are lower 1-2 orders of magnitude than that of the surrounding blocks based on Monlar and Tapponnier(1981)[37] (case 2-14, Table 1）. In addition, we run another numerical model where the lower crust has the same large viscosity 10^{28}Pa·s everywhere(case 1). This end-member case allows us to know about the importance of the lower crustal ductile flow well in explaining the interseimic elastic deformation of the upper crust.

Table 1 Models' parameters and results in the numerical experiments

Fig. 3a shows the root mean squares of the case 1-8 prediction errors of the velocity directions of the GPS stations. When the viscosity of the Tibetan lower crust is lower one order of magnitude than that of the surrounding crustal blocks, the model prediction errors decrease with the reduction of the Tibetan lower crustal viscosity. But for a distinct region, the trend of the prediction error change has some differences. In the Tibetan southeastern area（C area），the model prediction errors of the velocity directions of the GPS stations always decrease with the reduction of the Tibetan lower crustal viscosity. In the central-northern(A area) and northeastern(B area) areas of the Tibetan plateau, the model prediction errors decrease firstly, then alter to increase with the reduction of the Tibetan lower crustal viscosity when it is lower than 5×10^{22}Pa·s. This character is more obvious in the Tibetan central-northern area(Fig.3a）. These results imply that the actual viscosity of the Tibetan lower crust changed laterally, with its value in the southeastern area being much lower than that in the central-northern and northeastern areas of the Tibetan plateau. Ignoring the lateral change of the viscosity, the numerical experimental results suggest that the mean value of the Tibetan lower crustal viscosity might be between 10^{22}Pa·s and 5×10^{22}Pa·s.

Since the discrepancy between the lower crustal viscosity of the Tibetan plateau and that of the surrounding crustal blocks couldn't be specific, we perform the second (case 9-11) and third (case 12-14) groups of numerical experiments （Table 1）. The experimental results show that the same conclusion as above could be obtained even if the viscosity of the Tibetan lower crust is lower several decades or one hundred of times than that of the surrounding crustal blocks.

Note: $10^{24}/10^{23}$ denotes that the lower crustal viscosity value of the Tibetan plateau and that of the surrounding crustal blocks are 10^{24}Pa·s and 10^{23}Pa·s, respectively. $/10^{22}$ denotes that the viscosity of the deep fault zones is 10^{22}Pa·s, with the lower crustal viscosity of the whole model being about 10^{24}Pa·s. $//10^{22}$ denotes that the viscosity of the deep fault zones is 10^{22}Pa·s, with the lower crustal viscosity of the Tibetan plateau and that of the surrounding crustal blocks being about 2.5×10^{22}Pa·s and 10^{24}Pa·s, respectively. RMS means the root mean square of the model prediction errors of the values or directions of the GPS station velocities.

On the assumption that the viscosity of the Tibetan lower crust is 2.5×10^{22}Pa·s，being lower 40 times than that of the surrounding crustal blocks ,10^{24}Pa·s, the case 15 presents the lowest root mean square of the prediction errors of the velocity directions of the GPS stations in all the experiments having been done, with its value being about 18° in the central-northern and northeastern areas and being about 26° in the southeastern area of the Tibetan plateau（Table 1）.

Fig.3 Root mean square of the errors between GPS velocity directions and those predicted by numerical models.

a, models' prediction error versus the Tibetan lower crustal viscosity; b, models' prediction error versus the viscosity of deep fault zones; c, contrast of prediction errors of the models representing different geodynamic mechanisms; d, contrast of prediction errors of the models integrating the two geodynamic mechanisms together; e, effect of gravity on the prediction error. Triangle, solid circle and asterisk represent the errors of the central-northern area (A area), the northeastern area (B area) and the southeastern area (C area) of the Tibetan plateau, respectively. Diamond represents the total error of the model.

B. Effect of the shear strain localization in the deep fault zones on the Tibetan present-day crustal movement

On the contrary to the above experiments, ignoring the discrepancy of the viscosity of the Tibetan lower crust and that of the surrounding crustal blocks and supposing that the ductile flow of the Tibetan lower crust be very weak, with its viscosity value being about 10^{24}Pa·s, the case 16-19 are used to test the influence of the ductile shear strain localization in the Tibetan deep fault zones on the GPS velocity field, which is realized by adopting the different viscosities between the deep fault zones and their intermediate blocks here (Table 1）.

Fig. 3b shows that the model prediction errors are not sensitive to the change of the viscosity of the deep fault zones in the Tibetan northeastern area（B area），and however, both decrease firstly, then alter to increase with the reduction of viscosity value of the deep fault zones when it reduces to 10^{21}Pa·s in the central-northern （A area）and southeastern （C area）areas of the Tibetan plateau. The case 18, in which the viscosity value of the deep fault zones is 10^{21}Pa·s, presents the lowest root mean square of the prediction errors of the velocity directions of the GPS stations in this group of models (case 16-19), with its value being about 16° in the

central-northern and northeastern areas and being about 29° in the southeastern area of the Tibetan plateau.

Comparing case 18 with case 15（Fig. 3c）, it can be inferred that their corresponding geodynamical models about the lower crustal deformation have different suitability for a specific area of the Tibetan plateau. The GPS velocity field is accounted for better by the shear strain localization in the deep fault zones in the Tibetan central-northern and northeastern areas and by the ductile flow of the Tibetan lower crust in the Tibetan southeastern area, which can be seen more clearly by comparing the result of case 18 with that of case 12-15(Table 1).

C. Comprehensive explanation to the GPS velocity field

When ignoring the lateral change of the Tibetan lower crustal viscosity, the above numerical results reveal that the GPS velocity field is interpreted with a large error whether by the Tibetan lower crustal ductile flow or by the ductile shear strain localization in the deep fault zones separately, which is especially apparent in the Tibetan southeastern area. In order to improve the experimental result, suppose that both the Tibetan lower crustal ductile flow and the ductile shear strain localization in the deep fault zones affect the interseismic elastic strain accumulation in the upper crust so as to have an impact on the GPS velocity field, we carry out another group of numerical experiments, with the lower crustal viscosity of the Tibetan plateau and that of the surrounding crustal blocks being about 2.5×10^{22}Pa·s and 10^{24}Pa·s, respectively, and the viscosity of the deep fault zones varying between 10^{22}Pa·s and 5×10^{20}Pa·s（case 20-23, Table 1）.

Fig. 3d illustrates that the total prediction error of case 22, in which the viscosity of the deep fault zones is still about 10^{21}Pa·s, is lowest in this group of experiments. Compared with those cases that take either the Tibetan lower crustal ductile flow or the ductile shear strain localization in the deep fault zones individually, the root mean square of prediction errors of the velocity directions of the GPS stations in case 22 reduces to about 22° in the Tibetan southeastern area. It is especially remarkable that compared with case 18, in which only the ductile shear strain localization in the deep fault zones is involved, the root mean square of prediction errors of the velocity directions of the GPS stations in case 22 has some increase in the central-northern and northeastern areas of the Tibetan plateau (Fig.3c)，confirming that the shear strain localization in the deep fault zones affect the elastic deformation in upper crust stronger than the Tibetan lower crustal ductile strain in these regions.

Additionally, although the root mean square of prediction errors of the velocity directions of the GPS stations in case 22 reduces to about 22° in the Tibetan southeastern area., it is larger than that in the central-northern and northeastern areas of the Tibetan plateau in case 18. The lateral change of the lower crustal viscosity need to be taken into account so as to diminish the model prediction error[37] 。

V. DISCUSSION AND CONCLUSION

In this research, we test the effect of the Tibetan lower crustal ductile flow and that of the shear strain localization in the deep fault zones on the Tibetan present-day GPS velocity field, and find that they have different suitability in explaining the GPS data for a distinct area of the Tibetan plateau.

In the Tibetan southeastern area, although the shear strain localization in the deep fault zones could not be rejected by the experimental results, it is clear that the viscosity of the lower crust should be much lower in order to diminish the model's prediction error, implying that the ductile flow of the Tibetan lower crust facilitate the elastic strain accumulation in the upper crust in this area. The viewpoint of the weak lower crust in the southeast of the Tibetan plateau is in agreement with the opinion of Royden et al.(1997)[12] who proposed that in the central to southern area of the eastern Tibetan plateau, the lower crust is so weak that upper crustal deformation is decoupled from the motion of the underlying mantle, which has being affected the kinematics of this area since 4 Ma ago.

In the central-northern and northeastern areas of the Tibetan plateau, the GPS velocity field is interpreted much better by the ductile shear strain localization in the deep fault zones（Fig.3c）, suggesting that the actual active faults might incise down deeply in these areas. This suggestion is consistent with the point of view arisen from other data by someone else. With a seismic tomography study Wittlinger et al.(1998) suggested that the Altyn Tagh fault in the mantle is about 40 km wide and is continuous down to a depth of 140 km at least[38]. Shear-wave splitting measurements[39] above the Altyn Tagh fault show fast split shear waves polarized in a plane parallel to the trend of the fault and delay times between the fast and slow S-wave arrivals of about 1s. Such delay times require a thickness of anisotropic mantle of about 100km, in agreement with the value of fault penetration inferred from seismic tomography[14]. Approaching the Kunlun fault zone the orientation of the fast S-wave polarization plane progressively rotates into parallelism with the trend of the fault[40]，suggesting a shear strain gradient and an upper mantle fabric similar to that in the crust.

In addition, when the model integrates the shear strain localization in the deep fault zones and the Tibetan lower crustal ductile flow together, its prediction error increases a little. This phenomenon seems to not support the extensive ductile flow of the lower crust in the central- northern area(A area) of the Tibetan plateau. However, the magnitude of the error change is so low that this inference need to be tested by more detailed models.

Moreover, an uniform mean viscosity of the Tibetan lower crust, 10^{22}—5×10^{22}Pa·s, is obtained so as to account for the Tibetan present-day GPS velocity field with a first-order similarity. This result is close to the Tibetan lithospherical mean viscosity, 10^{22}Pa·s, given by England and Molnar(1997)[41] who ignored the elastic upper crust, and also in agreement with the value $0.5\text{-}5\times10^{22}$Pa·s calculated by Flesch et al.(2001)[42] according to the Tibetan strain rate as

well as the mean deviatonic stress field when ignoring the elastic upper crust. On the assumption that the Tibetan lower crustal mean viscosity is about 2.5×10^{22}Pa·s，the experiments yield an estimate of 10^{21}Pa·s for the mean viscosity of the deep fault zones.

With the above value of the Tibetan lower crustal viscosity, the influence of gravity on the Tibetan present-day GPS velocity field is also tested(Fig.3e). Obviously, the gravity has an important effect on the Tibetan present-day GPS velocity field, which is attributed to not only the Tibetan high elevation but also the lower viscosity of the Tibetan lower crust.

As a whole, the major conclusions could be summarized as follows:

1) The present-day crustal movement in the different regions of the Tibetan plateau may be attributed to the different geodynamic mechanisms. In the Tibetan southeastern area, although the shear strain localization in the deep fault zones could not be rejected, the viscosity of the lower crust should be much lower so as to diminish the model's prediction error. In the central-northern and northeastern areas of the Tibetan plateau, the GPS velocity field is accounted for better by the shear strain localization in the deep fault zones, implying that the actual active faults might incise down deeply in these areas.

2) Ignoring the lateral change of the Tibetan lower crustal viscosity, the preferred model which produces an approximation of the GPS velocity field with a a first-order similarity yields an estimate of 10^{22}—5×10^{22}Pa·s for the mean viscosity of the Tibetan lower crust, and at the same time an estimate of about 10^{21}Pa·s for that of the deep fault zones.

3) Due to the high elevation and the lower viscosity of the lower crust, the gravity plays an important role on the present-day movement of the Tibetan plateau.

REFERENCES

[1] P. Molnar, and H. Lyon-Caen, Fault plane solutions of earthquakes and active tectonics of the northern and eastern parts of the Tibetan Plateau, *Geophys. J. Int.* , Vol.***99,*** 1989, pp. 123-153.

[2] P. Molnar, and W. P. Chen, Focal depths and fault plane solutions of earthquakes under the Tibetan plateau, *Journal of Geophysical Research*, Vol.***88****(B2)*, 1983, pp. 1180-1196.

[3] W. Thatcher, Microplate versus continuum descriptions of active tectonic deformation, *Journal of Geophysical Research*, Vol.***100****(B3)*, 1995, pp. 3885-3894.

[4] S. J. Bourne, P. C. England, and B. Parsons, The motion of crustal blocks driven by flow of the lower lithosphere and implications for slip rates of continental strike-slip faults, *Nature*, Vol.*391,* 1998, pp. 655-659.

[5] J. Savage, and R. Burford, Accumulation of tectonic strain in California, *Bull. Seismol. Soc. Am.,* Vol.***60,*** 1970, pp. 1877-1896.

[6] W. Thatcher, Systematic inversion of geodetic data in central California, *Journal of Geophysical Research*, Vol.***84,*** 1979, pp. 2283-2295.

[7] W. Thatcher, Nonlinear strain buildup and the earthquake cycle on the San Andreas fault, *Journal of Geophysical Research*, Vol.***88,*** 1983, pp. 5893-5902.

[8] W. H. Prescott, and A. Nur, The accommodation of relative motion at depth on the San Andreas fault system in California, *Journal of Geophysical Research*, Vol.***86,*** 1981, pp. 999-1004.

[9] G. Houseman, and P. England, Finite strain calculations of continental deformation: method and general results for convergent zones, *Journal of Geophysical Research*, Vol.***91****(B3)**,* 1986, pp. 3651-3663.

[10] S. Lamb, Behavior of the brittle crust in wide plate boundary zones, *Journal of Geophysical Research*, Vol.*99(B1),* 1994, pp. 4457-4483.

[11] K. D. Nelson, W. J. Zhao, L. D. Brown,, J. Kuo, J. K. Che, X. W. Liu, et al., Partially molten middle crust beneath Southern Tibet: Synthesis of Project INDEPTH results, *Science*, Vol.***274,*** 1996, pp. 1684-1688.

[12] L. H. Royden, B. C. Burchfiel, R. W. King, E. Wang, Z. Chen, F. Shen, et al., Surface deformation and lower crustal flow in eastern Tibet, *Science*, Vol.***276***, 1997, pp. 788-790.

[13] M. D. Zoback, W. H. Prescott, and A. W. Krueger, Evidence for lower crustal ductile strain localization in southern New York, *Nature*, Vol.***317,*** 1985, pp. 705-707.

[14] A. Vauchez, and A. Tommasi, Wrench faults down to the asthenosphere: Geological and Geophysical evidence and thermo-mechanical effects, In: Storti, F., R. E. Holdsworth, and F. Salvini eds., Intraplate Strike-slip Deformation Belts, *London: Geological Society of London, Special Publication,* Vol. *210,* 2003, pp. 15-34.

[15] J. Dewey, R. M. Shackleton, C. Chang, and Y. Sun, The tectonic evolution of the Tibetan Plateau, *Philos. Trans. R. Soc. London, Ser. A*, Vol.***327****,* 1988, pp. 379-413.

[16] P. England, and G. Houseman, Finite strain calculations of continental deformation: comparison with the India-Asia collision zone, *Journal of Geophysical Research*, Vol.***91****(B3)**,* 1986, pp. 3664-3676.

[17] G. Houseman, and P. England, A lithospheric-thickening model for the Indo-Asian collision, In:Yin, A., and T. M. Harrison Eds., The Tectonic Evolution of Asia, *Cambridge: Cambridge University Press,* 1996, pp. 3-17.

[18] P. Tapponnier, G. Peltzer, AY. L. Dain, R. Armijo, P. Cobbold,, Propagating extrusion tectonics in Asia: new insights from simple experiments with plasticine, *Geology*, Vol.***10,*** 1982, pp. 611-616.

[19] G. Peltzer, and P. Tapponnier, Formation and evolution of strike –slip faults, rifts, and basins during the Indian-Asia collision: an experimental approach, *Journal of Geophysical Research*, Vol.***93,*** 1988, pp. 15,085-15,117.

[20] K. Y. Abdrakhmatov, S. A. Aldazhanov, B. H. Hager, M. W. Hamburger, T. A. Herring, K. B. Kalabaev, et al., Relatively recent construction of the Tien Shan inferred from GPS measurements of present-day crustal deformation rates, *Nature*, Vol.***384***, 1996, pp. 450-453.

[21] R. W. King, F. Shen, B. C. Burchfiel, L. H. Royden, E. Wang, Z. L. Chen, et al., Geodetic measurement of crustal motion in southwest China, *Geology*, Vol.25(2), 1997, pp. 179-182.

[22] K. M. Larson, R. Burgmann, R. Bilham, Jeffrey T. Freymueller, Kinematics of the India-Eurasia collision zone from GPS measurements, *Journal of Geophysical Research*, Vol.***104****(B1)**,* 1999, pp. 1077-1093.

[23] Z. Chen, B. C. Burchfiel, Y. Liu, R. W. King, L. H. Royden, W. Tang, et al., Global positioning system measurements from eastern Tibet and their implications for India/Eurasia intercontinental deformation, *Journal of Geophysical Research*, Vol.***105****(B7),** 2000, pp. 16,215-16,227.

[24] R. Bendick, R. Bilham, J. Freymueller, K. Larson, G. Yin, Geodetic evidence for a low slip rate in the Altyn Tagh fault system, *Nature*, Vol.***404,*** 2000, pp. 69-72.

[25] Z. K. Shen, M. Wang,, Y. X. Li, D. D. Jackson, A. Yin, D. Dong, et al., Crustal deformation along the Altyn Tagh fault system, western China,

from GPS, *Journal of Geophysical Research*, Vol.***106***（B12）, 2001, pp. 30607-30621.

[26] Q. Wang, P. Z. Zhang,, J. T. Freymueller, R. Bilham, K. M. Larson, X. Lai, et al., Present-day crustal deformation in China constrained by global positioning system measurements, *Science*, *294,* 2001,pp.574-577.

[27] P. Z. Zhang, Z. K. Shen, M. Wang, W. J. Gan, R. Burgmann, P. Molnar, Q. Wang, Z. J. Niu, J. Z. Sun, J. C. Wu, H. R. Sun, and X. Z. You, Continuous deformation of the Tibetan Plateau from global positioning system data, *Geology*, Vol.***32(9),*** 2004, pp. 809-812.

[28] R. Bilham, K. Larson, J. Freymueller, GPS measurements of present-da y convergence across the Nepal Himalaya, *Nature*, Vol.***386,*** 1997, pp. 61-64.

[29] R. Cattin, and J. P. Avouac, Modeling mountain building and the seismic cycle in the Himalaya of Nepal, *Journal of Geophysical Research*, Vol.***105***（B6）, 2000, pp. 13,389-13,407.

[30] J. P. Loveless, and M. Meade, Partitioning of localized and diffuse deformation in the TibetanPlateau from joint inversions of geologic and geodetic observations, *Earth and Planetary Science Letters,* Vol. *303(1–2)*, 2011, pp. 11–24.

[31] Q. D. Deng, P. Z. Zhang, Y. K. Ran, Principal features of the active tectonics in China, *Science in China(D)*(in Chinese), Vol.***32(12)***, 2002, pp. 1020-1030.

[32] Y. P. Wang, Principal features of the active tectonics in Qinghai-Xizang plateau, In: Ye, S. H. eds., Study on the Recent Deformation and Dynamics of the Lithosphere of Qinghai-Xizang Plateau(in Chinese), *Beijing: Seismological Press,* 2001, pp. 251-263.

[33] J. W. Teng, S. B. Xiong, and Z. J. Zhang, Review and prospects for geophysical study of the deep lithosphere structure and tectonics in Qinghai-Xizang(Tibet) Plateau, *Acta Geophysica Sinica(Supp.)* (in Chinese), Vol.***40,*** 1997, pp. 121-139.

[34] R. G. Gordon, D. F. Argus, and M. B. Heflin, Revised estimate of the angular velocity of India relative to Eurasia (Abstract), *EOS*, Vol.***80,*** 1999, pp. 273.

[35] W. F. Brace, and D. L. Kohlstedt, Limits on lithospheric stress imposed by laboratory experiments, *Journal of Geophysical Research*, Vol.***85(B11)***, 1980, pp. 6428-6252.

[36] S. P. Neves, A. Tommasi, A. Vauchez, and R. Hassani, Intraplate continental deformation: Influence of a heat-producing layer in the lithospheric mantle, Earth and Planetary Science Letters, vol.274(3–4), 2008, pp.392–400.

[37] P. Molnar, and P. Tapponnier, A possible dependence of tectonic strength on the age of the crust in Asia, *Earth and Planetary Science Letter*, Vol.***52,*** 1981, pp. 107-114.

[38] G. Wittlinger, P. Tapponnier, G. Poupinet, M. Jiang, D. N. Shi, G. Herquel, et al., Tomographic evidence for localized lithospheric shear along the Altyn Tagh fault, *Science*, Vol. ***282,***1998, pp. 74-76.

[39] G. Herquel, P. Tapponnier, G. Wittlinger, M. Jiang, D. N. Shi, Teleseismic shear wave splitting and lithospheric anisotropy beneath and across the Altyn Tagh fault, *Geophysical Research Letters*, Vol.***26***, 1999, pp. 3225-3228.

[40] D. E. McNamara, T. J. Owens, P. G. Silver, F. T. Wu, Shear wave anisotropy beneath the Tibetan Plateau, *Journal of Geophysical Research*, ***99,*** 1994, pp. 13,655-13,665.

[41] P. England, and P. Molnar, Active deformation of Asia：from kinematics to dynamics, *Science*, Vol.***278,*** 1997, pp. 647-650.

[42] L. M. Flesch, A. J. Haines, and W. E. Holt, Dynamics of the India-Eurasia collision zone, *Journal of Geophysical Research*, Vol.***106(B8)***, 2001, pp. 16,435-16,460.

APPENDIX

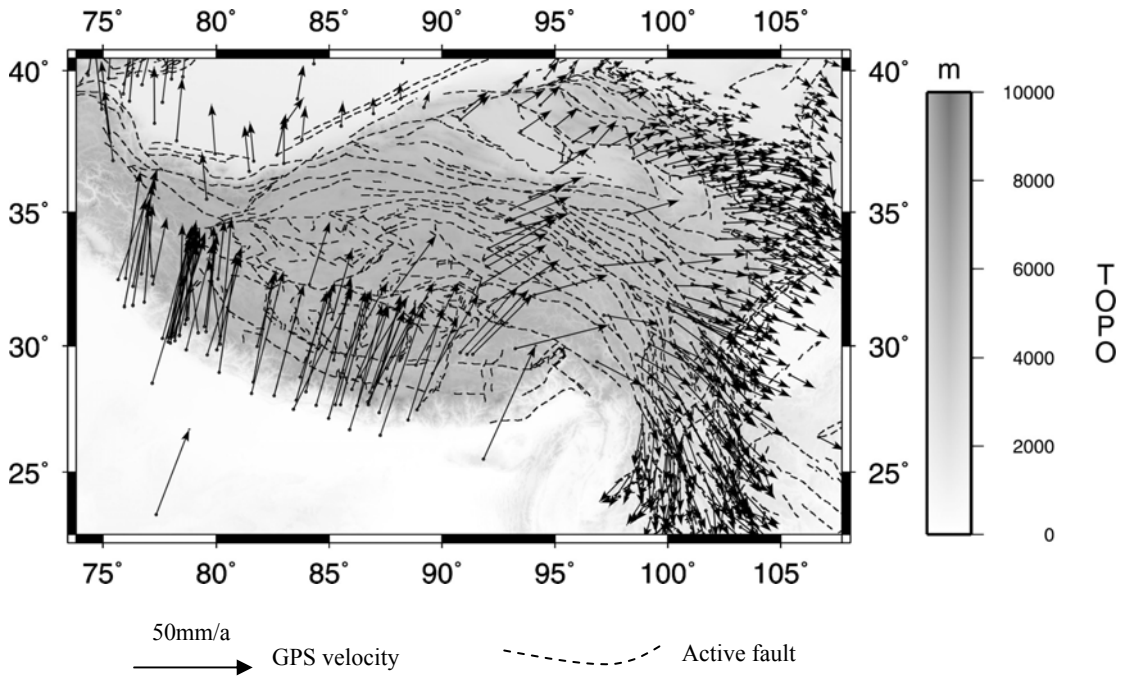

Fig.1 Simplified active tectonic map of the Tibetan plateau. The dashed curve lines show the locations of the active faults based on Deng et al.(2002). The straight lines shows the velocity vectors of the GPS stations referring to Zhang et al.(2004), and the raw data are obtained from http://www.geosociety.org/pubs/ft2004.htm. The shade of gray denotes the elevation according to the global ETOPO5 data.

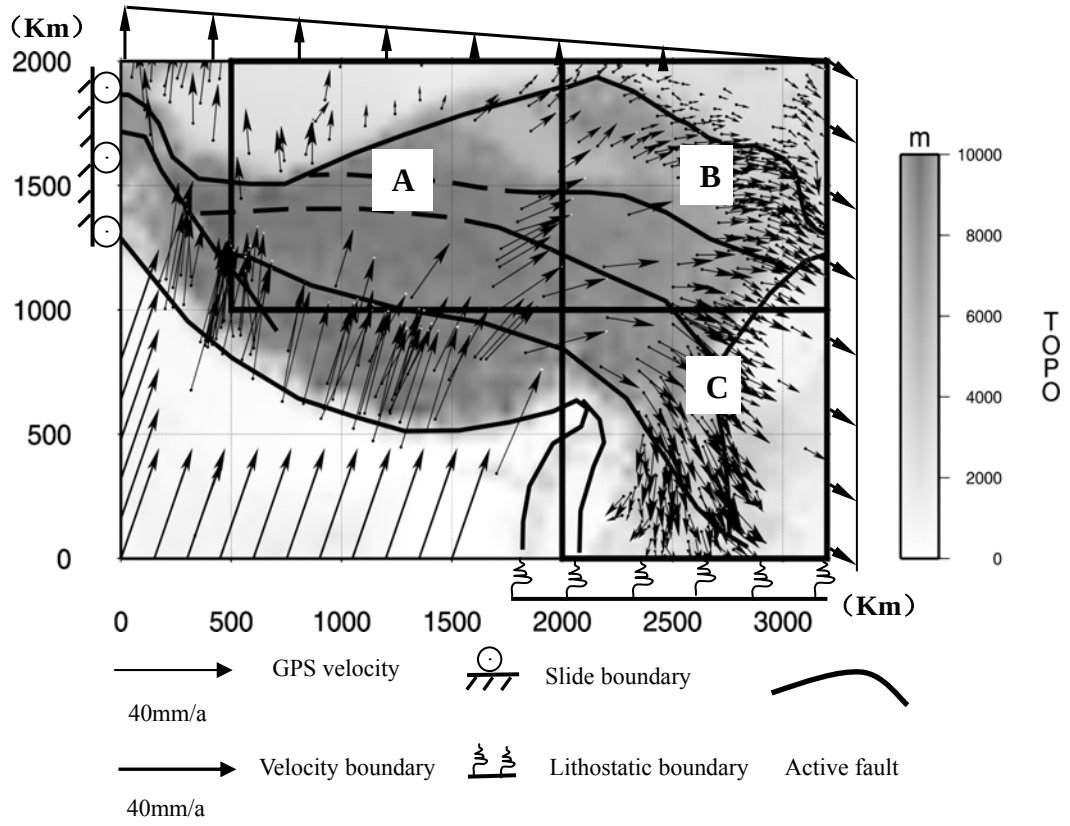

Fig.2 Geometry and boundary conditions of the mechanical model. The model covers the same area as that shown in Fig.1. The curve lines represent the major active faults. The thin and thick straight lines with an arrow represent the velocity vectors of the GPS stations and the velocity boundary conditions, respectively. The northwestern boundary is set to slide freely along the S-N direction,and is constrained along E-W direction. The southeastern boundary is subjected to the lithostatic pressure laterally. A, B and C represent three subareas, which are used to evaluate the model.

Table 1 Models' parameters and results in the numerical experiments

Case #	viscosity （Pa·S）	RMS in area A		RMS in area B		RMS in area C		Total RMS	
		Velocity (mm/yr)	***Direction (º)***	*Velocity (mm/yr)*	***Direction (º)***	*Velocity (mm/yr)*	***Direction (º)***	*Velocity (mm/yr)*	***Direction (º)***
1	**$10^{28}/10^{28}$**	**6.788**	**20.586**	**3.836**	**16.138**	**6.598**	**38.602**	**6.133**	**25.614**
2	$10^{27}/10^{26}$	6.706	**20.201**	3.785	**16.279**	7.153	**37.641**	6.353	**25.148**
3	$10^{26}/10^{25}$	6.700	**20.119**	3.779	**16.290**	7.284	**37.327**	6.411	**24.990**
4	$10^{25}/10^{24}$	6.732	**19.970**	3.770	**16.271**	7.234	**36.935**	6.414	**24.780**
5	$10^{24}/10^{23}$	7.105	**18.757**	3.772	**16.122**	6.847	**33.144**	6.514	**22.778**
6	**$5\times10^{23}/5\times10^{22}$**	**7.469**	**17.750**	**3.825**	**16.209**	**6.398**	**30.080**	**6.648**	**21.268**
7	$10^{23}/10^{22}$	8.542	**27.415**	5.759	**18.458**	3.309	**22.276**	8.340	**22.046**
8	$10^{22}/10^{21}$	13.785	**60.193**	19.189	**19.477**	14.684	**22.173**	17.640	**54.488**
9	**$10^{24}/5\times10^{22}$**	**7.464**	**17.756**	**3.807**	**16.203**	**6.409**	**30.053**	**6.637**	**21.256**
10	$5\times10^{23}/10^{22}$	8.470	**27.275**	5.424	**18.469**	3.341	**21.991**	8.070	**21.734**
11	$10^{23}/5\times10^{21}$	8.846	**38.293**	8.416	**19.639**	4.666	**20.732**	10.151	**28.349**
12	**$10^{24}/10^{22}$**	**8.476**	**27.275**	**5.375**	**18.479**	**3.355**	**21.917**	**8.033**	**21.685**
13	$5\times10^{23}/5\times10^{21}$	8.707	**38.011**	7.982	**19.673**	4.421	**20.595**	9.789	**27.697**
14	$10^{23}/10^{21}$	11.083	**52.107**	13.265	**19.274**	10.551	**20.486**	13.313	**34.287**
15	**$10^{24}/2.5\times10^{22}$**	**7.961**	**17.656**	**3.980**	**16.673**	**5.561**	**26.192**	**6.883**	**19.751**
16	$/10^{23}$	6.789	**19.639**	3.764	**16.203**	7.140	**36.227**	6.435	**24.385**
17	$/10^{22}$	7.213	**17.652**	3.789	**16.099**	6.473	**31.559**	6.590	**21.941**
18	**$/10^{21}$**	**6.932**	**16.118**	**3.419**	**16.034**	**6.134**	**28.523**	**6.305**	**20.468**
19	$/10^{20}$	6.623	**18.985**	3.652	**16.393**	7.054	**35.850**	6.279	**24.205**
20	$//10^{22}$	8.033	**18.490**	4.207	**16.879**	5.065	**24.773**	7.091	**19.475**
21	$//5\times10^{21}$	8.052	**19.537**	4.376	**17.016**	4.604	**23.762**	7.219	**19.420**
22	**$//10^{21}$**	**7.721**	**17.878**	**3.962**	**16.745**	**4.454**	**22.443**	**6.862**	**18.557**
23	$//5\times10^{20}$	7.671	**17.223**	3.896	**16.573**	5.176	**24.637**	6.705	**19.060**

Note: $10^{24}/10^{23}$ denotes that the lower crustal viscosity value of the Tibetan plateau and that of the surrounding crustal blocks are 10^{24}Pa·s and 10^{23}Pa·s, respectively. $/10^{22}$ denotes that the viscosity of the deep fault zones is 10^{22}Pa·s, with the lower crustal viscosity of the whole model being about 10^{24}Pa·s. $//10^{22}$ denotes that the viscosity of the deep fault zones is 10^{22}Pa·s, with the lower crustal viscosity of the Tibetan plateau and that of the surrounding crustal blocks being about 2.5×10^{22}Pa·s and 10^{24}Pa·s, respectively. RMS means the root mean square of the model prediction errors of the values or directions of the GPS station velocities.

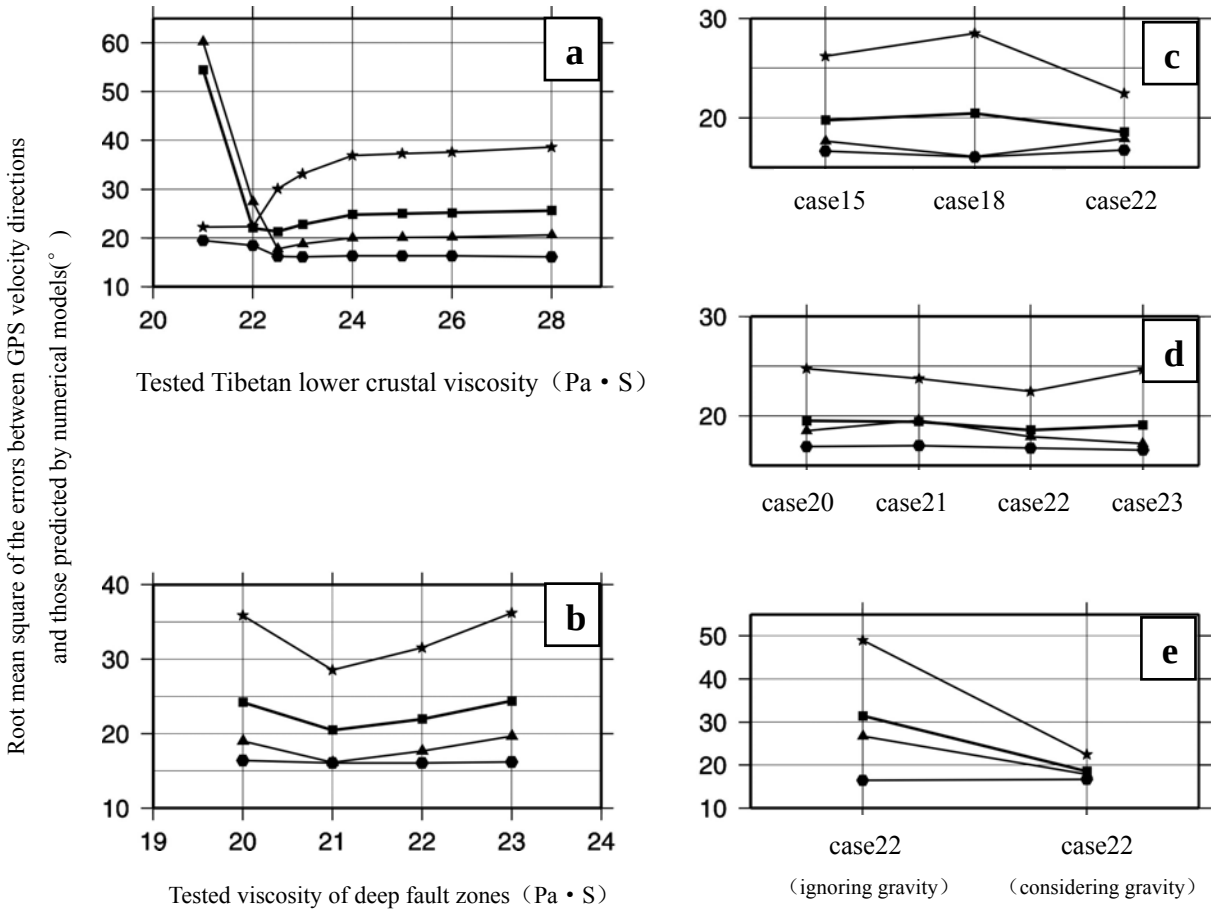

Fig.3 Root mean square of the errors between GPS velocity directions and those predicted by numerical models.
a, models' prediction error versus the Tibetan lower crustal viscosity; b, models' prediction error versus the viscosity of deep fault zones; c, contrast of prediction errors of the models representing different geodynamic mechanisms; d, contrast of prediction errors of the models integrating the two geodynamic mechanisms together; e, effect of gravity on the prediction error. Triangle, solid circle and asterisk represent the errors of the central-northern area (A area), the northeastern area (B area) and the southeastern area (C area) of the Tibetan plateau, respectively. Diamond represents the total error of the model.

LU SHIKUO~ School of Geosciences, China University of Petroleum(East China), Qingdao City, Shandong Province, China; LSKUO@sina.com

LU Shikuo is an Associate Professor at the China University of Petroleum (East China), who joined the university after three years as a Postdoctor in the Institute of Tibetan Plateau Research, Chinese Academy of Science. He holds a Ph.D. in Geodynamics from Peking University, China(2004). His current research interests include the deformation of continental collision, structure in sedimentary basins and the diagenesis in fault zones.